# Pentacoordinate ($\mu$-Oxo)diiron(III) Thiolate Complexes and Dimeric Iron(II) Precursors

**Ghezai Musie, Chia-Huei Lai, Joseph H. Reibenspies, Lloyd W. Sumner, and Marcetta Y. Darensbourg***

Department of Chemistry, Texas A&M University, College Station, Texas 77843

*Received April 28, 1998*

The ($\mu$-oxo)diiron(III) complexes of *N*,*N*′-bis(2-methyl-2-mercaptopropane)-1,5-diazacyclooctane ($H_2$bme*-daco) and *N*,*N*′-bis(mercaptoethyl)-1,5-diazacyclooctane ($H_2$bme*-daco) ligands present uncommon examples of well-characterized ($\mu$-oxo)diiron(III) species in the presence of sulfur donors. Whereas the reaction of molecular oxygen with a solution of diiron(II) complex, [(bme*-daco)Fe]$_2$, affords slow formation of the $\mu$-oxo species, the presence of $O_2$ in the reaction of free ligand with the iron source, Fe(acac)$_3$, gave good yields in shorter time. With the less sterically encumbered derivative, [(bme-daco)Fe]$_2$, the only successful route to [(bme-daco)Fe]$_2$O required single O-atom sources such as 4-chloropyridine *N*-oxide to be present during the preparation of the complex; attempted use of molecular $O_2$ either during the synthesis or following isolation of the iron(II) dimer [(bme-daco)Fe]$_2$ resulted in decomposition. That is, both the reactant [(bme-daco)Fe]$_2$ and the product [(bme-daco)-Fe]$_2$O are unstable toward $O_2$. The molecular structures of [(bme*-daco)Fe]$_2$, [(bme*-daco)Fe]$_2$O, and [(bme-daco)Fe]$_2$O were determined by X-ray crystallography. The topological description of the Fe(II) dimers is that of edge-bridged square pyramids, with the Fe(II) displaced from the $N_2S_2$ planes of each ligand on average by 0.59 Å and engaged in a planar $Fe_2S_2$ core. For the ($\mu$-oxo)diiron(III) compounds, the square pyramids are O-vertex bridged, and the Fe(III) dome effect is 0.65 and 0.62 Å for [(bme*-daco)Fe]$_2$O and [(bme-daco)Fe]$_2$O, respectively. Further characterization by ESI mass spectroscopy, cyclic voltammetry, and EPR spectroscopy (of the one-electron reduced [(bme*-daco)Fe]$_2$O is presented. There was no indication of the ligand-based oxygen capture producing S-oxygenates which are prevalent in nickel derivatives of bme-daco and bme*-daco.

## Introduction

The *N*,*N*′-bis(mercaptoethyl)-1,5-diazacyclooctane ($H_2$-bme-daco) ligand and a sterically encumbered analogue, *N*,*N*′-bis-(2-methyl-2-mercaptopropane)-1,5-diazacyclooctane ($H_2$-bme*-daco), have provided monomeric square planar $Ni^{II}$ and $Pd^{II}$ complexes which show extensive S-site reactivity including oxygenation with both $H_2O_2$ and molecular $O_2$. For M = Ni metallosulfoxides or M−S(=O)R predominate for oxygenates of bme*-daco, while sulfones (M−$SO_2$R) are more stable for the parent bme-daco.[1] The metric data from 15 molecular structures determined by X-ray crystallography showed minor differences in Ni−S and Pd−S bond lengths with varying levels of S-oxygenation in the (bme-daco)$M^{II}$ and (bme*-daco)$M^{II}$ derivatives, while $M^{II/I}$ redox couples became systematically more accessible with each added oxygen atom. Such oxygen modification of a bound donor site leading to redox differences in a complex whose coordination geometry is intact is of significance to sulfur-rich catalytic sites whose activity might be regulated by electronic effects. The possibility of utilizing S-oxygenation as a trap for $^3O_2$ and $^1O_2$ is also interesting in view of the applications of metal thiolates as antioxidants for olefin stabilization.[2] While the maximum O-storage power of our $N_2S_2$ complexes is four O-atoms, a less rigid ligand, $H_2$-dsdm, takes up three O-atoms per thiolate sulfur, forming a 6-oxy, O-bound disulfonate.[3]

The abundance of sulfur-rich iron moieties in biology encouraged a search for similar S-based oxygen uptake reactivity of iron thiolates. That iron sulfinates might be stable is presaged by the organometallic ($\eta^5$-$C_5H_5$)Fe(CO)$_2$($SO_2$R), prepared by $SO_2$ insertion into ($\eta^5$-$C_5H_5$)-Fe(CO)$_2$(R).[4] On the other hand, iron-site oxygen uptake with formation of ($\mu$-oxo)diiron(III) complexes is a common reaction, especially in nitrogen and oxygen donor environments.[5] While many are in octahedral arrays with the $\mu$-oxo bridges supported by other bridging ligands, a search of >140 000 entries in the Cambridge Crystal Structure Database (CSD) found ca. 30 hits for unsupported pentacoordinate ($\mu$-oxo)diiron(III) complexes.[6] All such complexes, many with porphyrin and Schiff-base type ligands, find $Fe^{III}$ displaced by an average of 0.54 Å from the $L_4$ plane toward the bridging O. Additional interest in this structural form arises

(1) (a) Mills, D. K.; Hsiao, Y. M.; Farmer, P. J.; Atnip, E. V.; Reibenspies, J. H.; Darensbourg, M. Y. *J. Am. Chem. Soc.* **1991**, *113*, 1421. (b) Mills, D. K. Ph.D. Dissertation, Texas A&M University, College Station, TX, 1991. (c) Tuntulani, T. Ph.D. Dissertation, Texas A&M University, College Station, TX, 1995.

(2) (a) Carlsson, D. J.; Suprunchuk, T.; Wiles, D. M. *J. Polym. Sci., Part B: Polym. Lett.* **1973**, *11*, 61. (b) Monroe, B. M.; Mrowca, J. J. *J. Phys. Chem.* **1979**, *83*, 591. (c) Furue, H.; Russell, K. E. *Can. J. Chem.* **1978**, *56*, 1595.

(3) $H_2$dsdm = *N*,*N*′-dimethyl-*N*,*N*′-bis($\beta$-mercaptoethyl)ethylenediamine; Henderson, R. K.; Bouwman, E.; Spek, A. L.; Reedijk, J. *Inorg. Chem.* **1997**, *36*, 4616.

(4) Wojcicki, A. *Adv. Organomet. Chem.* **1974**, *12*, 31.

(5) (a) Hoffman, A. B.; Collins, D. M.; Day, V. W.; Fleischer, E. B.; Srivastava, T. S.; Hoard, L. H. *J. Am. Chem. Soc.* **1972**, *94*, 3620. (b) Schugar, H. J.; Rossmann, G. R.; Barraclough, C. G.; Gray, H. B. *J. Am. Chem. Soc.* **1972**, *94*, 2683. (c) Lippard, S. J.; Schugar, H.; Walling, C. *Inorg. Chem.* **1967**, *6*, 1825. (d) Ercolani, C.; Gardini, M.; Monacelli, F.; Pennesi, G.; Rossi, G. *Inorg. Chem.* **1983**, *22*, 2584.

(6) Allen, F. H.; Davies, J. E.; Galloy, J. J.; Johnson, O.; Kennard, O.; Macrae, C. F.; Mitchell, E. M.; Mitchell, G. F.; Smith, J. M.; Watson, D. G. J. *Chem. Inf. Comput. Sci.* **1991**, *31*, 187. These results are obtained from metric data compiled from Cambridge Crystal Structure Database (CSD) for pentacoordinated ($\mu$-oxo)diiron(III) species.

S0020-1669(98)00475-3 CCC: $15.00 
Published on Web 07/25/1998

**Chart 1**

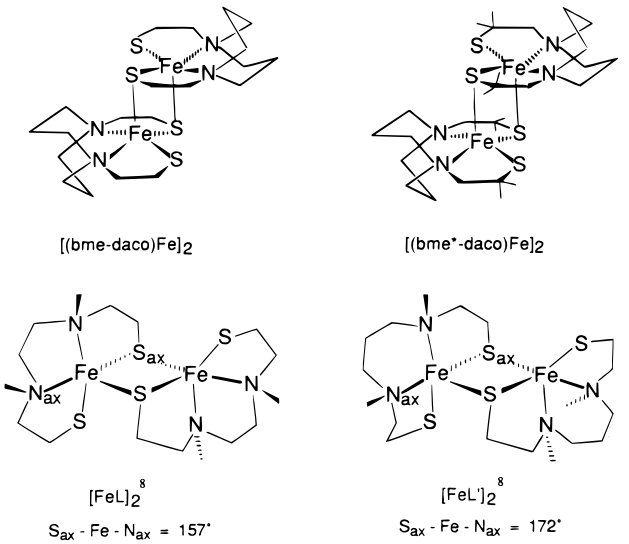


in the angularity of the Fe−O−Fe arrangement which ranges from 144 to 180°.[6] To date, no fully characterized (μ-oxo)-diiron(III) complex containing a sulfur donor(s) has been found, with the exception of a thiosalen tetradentate ($N_2S_2$) ligand derivative, whose crystal structure was partially determined by West and co-workers in 1983.[7]

The study below was designed to utilize the bme-daco and bme*-daco complexes of iron(II) which we reasoned should give maximum opportunity for the formation of S-oxygenates, and test relative oxygen affinity of Fe vs S. The structure of the former, [(bme-daco)Fe]$_2$, was previously determined to have an $Fe_2S_2$ core with equivalent Fe−S distances,[1a] consistent with its thermodynamically robust character. As shown below, the bme*-daco derivative is also a dimeric [(bme*-daco)Fe]$_2$ complex with core $Fe_2S_2$ metric data identical to that in [(bme-daco)Fe]$_2$. Each dimer has two terminal thiolates. Differences arise from the (limited) flexibility of the less sterically encumbered ligand, which is over-oxidized by molecular oxygen, yielding uncharacterized iron(III) products and ligand disulfides. Similar reactivity was previously seen in the open chain $N_2S_2$ ligand derivatives [FeL]$_2$ ($LH_2$ = *N*,*N*′-dimethyl-*N*,*N*′-bis(2-mercaptoethyl)ethylenediamine) and [FeL′]$_2$ ($L'H_2$ = *N*,*N*′-dimethyl-*N*,*N*′-bis(2-mercaptoethyl)-1,3-propanediamine) shown in Chart 1.[8] In contrast, as demonstrated below, the [(bme*-daco)Fe]$_2$ undergoes O-capture in the presence of $O_2$, not by sulfur, but iron, yielding the μ-oxo compound, [(bme*-daco)-Fe]$_2$O. Synthetic routes to the analogous [(bme-daco)Fe]$_2$O necessitated careful stoichiometric control of single O-atom sources.

It has been repeatedly shown that, in less sterically hindered ligands, the strong affinity of iron toward thiolate sulfurs produces stable aggregates of bi- and polymetallics.[8,1a] The powerful ability of the μ-oxo to bridge iron, exceedingly important in biological systems,[9] is demonstrated in our study to replace two μ-thiolates in a strong $Fe_2(SR)_2$ core, retaining binuclearity and ligand integrity in the course of oxidation of Fe(II) to Fe(III).

## Experimental Section

**General Methods.** Reagent grade solvents were dried and purified before use according to published procedures.[10] The Fe(acac)$_3$ was purchased from Strem Chemical Company; all other chemicals were purchased from Aldrich Chemical Co. and used as received. Where anaerobic conditions were required, standard Schlenk techniques using argon or $N_2$ (passed through a drying tube of $CaSO_4$, molecular sieves and NaOH), and an argon glovebox were employed. Elemental analysis were carried out by Galbraith Laboratories (Knoxville, TN).

**Physical Measurements.** UV−Vis spectra were recorded on a Hewlett-Packard HP8452A diode array spectrophotometer. EPR spectra were recorded on a Bruker ESP 300 equipped with an Oxford ER910A cryostat operating at 100 K. An NMR gaussmeter (Bruker ERO35M) and Hewlett-Packard frequency counter (HP5352B) were used to calibrate the field and microwave frequency, respectively. Samples, 0.15 mM in analyte, were frozen in liquid nitrogen prior to recording the EPR spectra.

Electrochemical measurements were made on a BAS-100A electroanalyzer controlled with an Intel 486DX computer and utilizing three-electrodes: glassy carbon or Pt working electrode, platinum wire counter electrode, and a Vycor-tipped Ag/$AgNO_3$ reference electrode. Working electrodes were polished to a mirror finish on a microcloth of diamond or alumina (1.0 and 0.05 mm particles, respectively) and were cleaned electrochemically. Data were analyzed by the software provided with this instrumentation. Cyclic voltammograms were obtained from 2.5 mM analyte concentration in $CH_3CN$, using 0.1 M [*n*-$Bu_4N$][$PF_6$] (TBAHFP) supporting electrolyte. Solutions were degassed with a purge of $N_2$ for 5 min; a blanket of $N_2$ was maintained over the solution while making the measurements. The *iR* compensation between the working and reference electrodes was accomplished by applying the positive feedback from the BAS-100A current follower. All potentials were scaled to NHE using ferrocene as an internal standard ($Cp_2Fe^+/Cp_2Fe$ literature value is $E_{1/2}^{NHE}$ = 400 mV in acetonitrile).[11]

The X-ray crystal structures were solved at the Crystal & Molecular Structure Laboratory Center for Chemical Characterization and Analysis at Texas A&M University. X-ray crystallographic data were obtained on a Siemens R3m/V single-crystal X-ray diffractometer operating at 55 kV and 30 mA, Mo Kα ($\lambda$ = 0.710 73 Å) radiation equipped with a Siemens LT-2 cryostat. Diffractometer control software P3VAX 3.42 was supplied by Siemens Analytical Instruments, Inc. All crystallographic calculations were performed with use of the Siemens SHELXTL-PLUS program package.[12] The structures were solved by direct methods. Anisotropic refinement for all non-hydrogen atoms was done by a full-matrix least-squares method. A single crystal was mounted on a glass fiber with epoxy cement either at room temperature or at 163 K in an $N_2$ cold steam. Cell parameter and data collection summaries for compounds [(bme*-daco)Fe]$_2$, [(bme*-daco)Fe]$_2$O, and [(bme-daco)Fe]$_2$O are given in Table 1.

Fast atom bombardment (FAB) mass spectra were acquired on a VG Analytical 70S (Manchester, U.K.) high-resolution, double-focusing, magnetic sector mass spectrometer equipped with a VG 11/250J data system to allow computer control of the instrument, data recording, and data processing. Samples for analysis were prepared by dissolving approximately 1 mg of analyte in 50 μL of methanol (solvent), from which 2 μL of this solution were mixed with approximately 3 μL of the *m*-nitrobenzyl alcohol (NBA) matrix and placed on the direct insertion probe tip. The probe was then inserted into the instrument through a vacuum interlock. The sample was bombarded with 8 keV Xenon primary particles from an Ion Tech FAB gun operating at an emission current of 2 mA. Positive secondary ions were extracted and accelerated to 6 keV and mass analyzed.

(7) Marini, P. J.; Berry, K. J.; Murray, K. S.; West, B. O. *J. Chem. Soc., Dalton Trans.* **1983**, 879.
(8) (a) Hu, W. J.; Lippard, S. J. *J. Am. Chem. Soc.* **1974**, *96*, 2366. (b) Karlin, K. D.; Lippard, S. J. *J. Am. Chem. Soc.* **1976**, *98*, 6951.
(9) (a) Que, L., Jr.; True, A. E. *Prog. Inorg. Chem.* **1990**, *38*, 97−200. (b) Feig, A. L.; Lippard, S. J. *Chem. Rev.* **1994**, *94*, 759−805.
(10) Gordon, A. J.; Ford, R. A. *The Chemist's Companion*; Wiley and Sons: New York, 1972; pp 429−436.
(11) Gagne, R. R.; Koval, C. A.; Lisensky, G. C. *Inorg. Chem.* **1980**, *19*, 2854.
(12) Sheldrick, G. *SHELXTL-PLUS*: *Program for Crystal Structure Refinement*; Institüt für Anorganische Chemie der Universität Göttingen: Göttingen, Germany, 1990.

**Table 1.** Crystallographic Summary for Structures $[(bme^*\text{-}daco)Fe]_2$, $[(bme^*\text{-}daco)Fe]_2O$, and $[(bme\text{-}daco)Fe]_2O$

| | $[(bme^*\text{-}daco)Fe]_2\cdot 2C_7H_8$ | $[(bme^*\text{-}daco)Fe]_2O\cdot C_7H_8$ | $[(bme\text{-}daco)Fe]_2O\cdot 2CH_2Cl_2$ |
|---|---|---|---|
| empirical formula | $C_{42}H_{72}Fe_2N_4S_4$ | $C_{35}H_{64}Fe_2N_4OS_4$ | $C_{22}H_{44}Fe_2N_4S_4OCl_4$ |
| fw (g/mol) | 872.9 | 796.85 | 762.35 |
| temperature, K | 153(2) | 293(2) | 203(2) |
| wavelength, Å | 0.71073 | 0.710 73 | 1.541 78 |
| crystal system | monoclinic | monoclinic | triclinic |
| space group | $P2(1)/c$ | $P2(1)/c$ | $P\bar{1}$ |
| unit cell dimensions | $a = 14.694(3)$ Å; $\alpha = 90°$<br>$b = 11.077(2)$ Å; $\beta = 104.499(9)°$<br>$c = 13.986(3)$ Å; $\gamma = 90°$ | $a = 12.086(2)$ Å; $\alpha = 90°$<br>$b = 14.888(3)$ Å; $\beta = 104.77(3)°$<br>$c = 11.499(2)$ Å; $\gamma = 90°$ | $a = 8.522(2)$ Å; $\alpha = 86.84(3)°$<br>$b = 8.540(2)$ Å; $\beta = 73.94(3)°$<br>$c = 12.207(2)$ Å; $\gamma = 71.60(3)°$ |
| volume, Å$^3$ | 2204.0(7) | 2000.7(7) | 809.5(3) |
| $Z$ | 4 | 2 | 1 |
| $\rho$ calculate, g/cm$^3$ | 1.315 | 1.236 | 1.564 |
| abs coeff, mm$^{-1}$ | 0.882 | 0.961 | 12.827 |
| $S(F^2)$[a] | 1.003 | 1.054 | 1.002 |
| abs. corr | $\psi$ scans | none | DIFABS |
| R($F$) [$I > 2\sigma(I)$],[a] % | 6.52 | 8.04 | 7.23 |
| wR($F^2$) all data,[a] % | 17.40 | 25.97 | 23.05 |

[a] Residuals: $R(F) = \sum|F_o - F_c|/\sum F_o$; $wR(F^2) = \{\sum w(|F_o^2| - |F_c^2|)^2/[\sum w(F_o^2)^2]\}^{1/2}$.

Electrospray ionization (ESI) mass spectra were acquired using a Vestec 201A quadrupole mass spectrometer (PerSeptive Biosystems/Vestec Mass Spectrometry Products, Framington, MA).[13,14] Mass spectra were recorded on a Technivent Vector One data system (Technivent Corp, Maryland Heights, MO) interfaced with an IBM-compatible Pentium personal computer. ESI was achieved with a stainless steel needle (250 $\mu$m o.d. × 125 $\mu$m i.d., and 0.75 in. long) maintained at a potential of approximately 2.0−2.4 kV. Analyte solutions (1 $\mu$g/$\mu$L in methanol) were injected via a Valco C14W, 1 $\mu$L internal loop injector (Valco Instrument Co., Houston, TX) into a mobile phase of 100% dry methanol supplied by a SAGE Instruments model 341B syringe pump (Orion Research Inc, Boston, MA) at a flow rate of 1.6 $\mu$L/min.

**Syntheses: $[(bme^*\text{-}daco)Fe]_2$.** Under an Ar atmosphere, a red toluene solution of $Fe(acac)_3$ (0.896 g, 2.5 mmol) was added dropwise to a toluene solution of $H_2$-bme*-daco ligand[15] (2.21 g, 7.5 mmol), i.e., a 1:3 mole ratio. The yellow color which immediately developed persisted for a few seconds and then turned brown. On stirring overnight a light red/brown powder of $[(bme^*\text{-}daco)Fe]_2$ settled; it was filtered, washed thoroughly with ether, and dried in air. The yield was 67% based on $Fe(acac)_3$. Crystals suitable for crystallographic analysis were grown by slow ether diffusion into a concentrated methanol solution of $[(bme^*\text{-}daco)Fe]_2$. Anal. Calcd (found) for ($Fe_2S_4N_4C_{28}H_{56}$): C, 49.2 (48.8); H, 8.22 (8.22); N, 7.45 (8.13). UV−vis in $CH_3OH$, $\lambda_{max}$, $\epsilon$(cm$^{-1}$ M$^{-1}$): 286 (8041), 412 (sh), 502 (sh). FAB-MS, $m/z$ (% intensity): 344 (17), 289 (12), 254 (5), 181 (5), 154 (15), 137 (100).

**$[(bme^*\text{-}daco)Fe]_2O$.** (a) Inside an Ar-filled glovebox, a 1.90 g (6.4 mmol) portion of $H_2$-bme*-daco was weighed into a 250 mL Schlenk flask containing 100 mL of toluene. In a separate flask 1.16 g (3.2 mmol) of $Fe(acac)_3$ was dissolved in 50 mL of toluene. Both flasks were removed from the glovebox, and with a 1:1 $O_2$/Ar stream constantly flowing, the $Fe(acac)_3$ solution was transferred dropwise by cannula into the ligand solution, over a period of ca. 20 min. The resulting deep brown solution was capped under a positive pressure of $O_2$/Ar and stirred overnight. The air-stable dark brown powder which resulted was filtered, washed with ether, and dried in air (0.91 g, ca. 80% yield based on $Fe(acac)_3$). Crystals developed when, following the mixing of reagents under $O_2$/Ar, the reaction solution was capped and allowed to stand undisturbed for several days.

(b) A methanol solution of $[(bme^*\text{-}daco)Fe]_2$ (100 mg, 145 mmol in 20 mL MeOH) in a 500 mL round-bottom flask was purged with $O_2$ for 30 min and kept under positive $O_2$ pressure for 1 week. On removal of the solvent under vacuum a dark brown solid, in ca. 10% yield, was obtained and was contaminated with ligand disulfide. X-ray-quality crystals of $[(bme^*\text{-}daco)Fe]_2O$ were obtained by slow (typically requiring 1 week) hexane diffusion into a saturated methanol solution.

Anal. Calcd (found) for ($Fe_2S_4N_4OC_{35}H_{64}$): C, 52.8 (52.8); H, 8.38 (8.01); N, 7.03 (6.14). UV−vis in $CH_3OH$, $\lambda_{max}$, $\epsilon$(cm$^{-1}$ M$^{-1}$): 314 (7259), 412 (sh), 502 (sh). FAB-MS, $m/z$ (% intensity): 705 (19), 485 (10), 404 (24), 344 (30), 202 (19), 137 (100), 115 (16).

Both $[(bme^*\text{-}daco)Fe]_2$ and $[(bme^*\text{-}daco)Fe]_2O$ are soluble in polar solvents such as methanol, acetonitrile, pyridine, tetrahydrofuran, and water and slightly soluble in nonpolar solvents such as hexane, benzene, toluene, and ether.

**$[(bme\text{-}daco)Fe]_2O$.** With minimal light inside a glovebox, a 0.350 g (1.5 mmol) portion of $H_2$-bme-daco was weighed into a 50 mL Schlenk flask wrapped in aluminum foil, which contained 0.065 g (0.5 mmol) of 4-chloropyridine *N*-oxide (light sensitive). A separate flask, charged with a 0.177 g (0.5 mmol) portion of $Fe(acac)_3$, was removed from the glovebox, and 20 mL of $CH_2Cl_2$ was added by syringe. The Schlenk flask containing the free ligand and the 4-chloropyridine *N*-oxide was also removed from the glovebox and slowly transferred into the $Fe(acac)_3$ solution by cannula in darkness. The colorless ligand solution slowly turned dark brown-purple. The resulting solution was concentrated by vacuum removal of solvent almost to dryness and with addition of ether (ca. 35 mL), a slightly air-sensitive dark brown precipitate formed. It was filtered anerobically, washed with ether, and dried. The crude product was dissolved in a minimum amount of $CH_2Cl_2$, in which it is extremely air sensitive, and X-ray-quality crystals were obtained by ether diffusion, yield of 23% based on the $Fe(acac)_3$. The crystals were very soluble in $CH_2Cl_2$, slightly soluble in methanol and insoluble in hexane, benzene, toluene, and ether.

Anal. Calcd (found) for ($Fe_2S_4N_4OC_{20}H_{40}\cdot CH_2Cl_2$): C, 40.5 (39.9); H, 6.81 (6.14); N, 9.46 (8.63). UV−vis in $CH_2Cl_2$, $\lambda_{max}$, $\epsilon$(cm$^{-1}$ M$^{-1}$): 284 (14 759), 322 (15 140), 416 (7558), 496 (sh, 5564). FAB-MS, $m/z$ (% intensity): 881 (47), 655 (73), 593 (54), 465 (52), 288 (100), 233 (96).

## Results and Discussion

**Synthesis.** The $[(bme^*\text{-}daco)Fe]_2$ and $[(bme^*\text{-}daco)Fe]_2O$ compounds were prepared by the routes given in Scheme 1; details are given in the Experimental Section. The $[(bme\text{-}daco)Fe]_2$ complex was similarly prepared from $Fe(acac)_3$, utilizing a portion of the dithiol ligand as a sacrificial reductant.[1a] Scheme 1 does not, however, apply to the synthesis of $[(bme\text{-}daco)Fe]_2O$, as the $[(bme\text{-}daco)Fe]_2$ compound and the $\mu$-oxo product decompose in the presence of $O_2$. Hence, the synthesis and isolation of the $[(bme\text{-}daco)Fe]_2O$ required use of the single O-donor reagent, 4-chloropyridine *N*-oxide, as shown in eq 1. At no point in the reactions were products with infrared bands

(13) Allen, M. H.; Vestal, M. L. *J. Am. Soc. Mass Spectrom.* **1992**, *3*, 18.
(14) Allen, M. H.; Field, F. H.; Vestal, M. L. In *Proceedings of the 38th Annual American Society for Mass Spectrometry Conference on Mass Spectrometry and Allied Topics*, Tucson, AZ, 1990; ASMS: Santa Fe, NM, 1990; p 431.
(15) Darensbourg, M. Y.; Font, I.; Pala, M.; Reibenspies, J. H. *J. Coord. Chem.* **1994**, *32*, 39.

**Scheme 1**

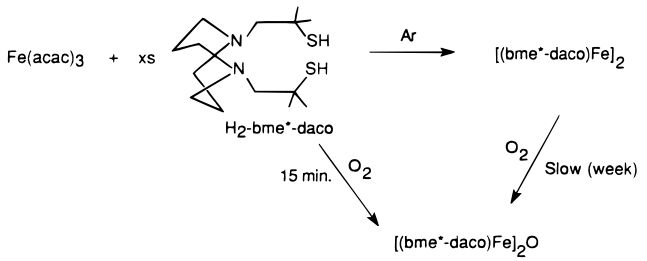


in the metallosulfoxide or metallosulfone region (950−1200 $cm^{-1}$) observed; the products showed the characteristic Fe−O−Fe bands in the 825−850 $cm^{-1}$ region.

The physical properties of the new compounds are given in the Experimental Section. All are orange-brown solids. Once isolated, the bme*-daco derivatives require no special handling in solid state, however the [(bme-daco)Fe]$_2$O compound is air-sensitive both in the solid state and in solution. Note that the one pot synthesis of the μ-oxo compound via the reaction in eq 1 does not require isolation of the [(bme-daco)Fe]$_2$ dimer as an

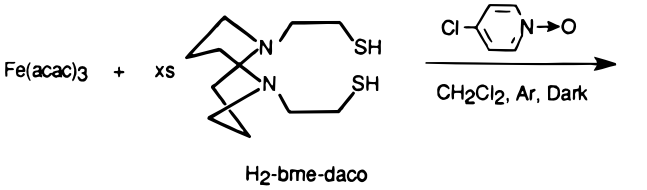


(1)

intermediate. In fact, the reaction of the isolated dimer with 4-chloropyridine *N*-oxide resulted in decomposition which remains uncharacterized.

**Molecular Structures: [(bme*-daco)Fe]$_2$.** The compound [(bme*-daco)Fe]$_2$ crystallizes in space group $P2_1/c$ of the monoclinic system with four molecules per unit cell. Four toluene solvent molecules cocrystallized with the iron complex. Selected metric data are given in Table 2, along with comparison to the structures of [(bme-daco)Fe]$_2$,[1a] and the μ-oxo complexes, *vide infra*. For the almost identical $Fe^{II}$ dimers, [(bme*-daco)-Fe]$_2$ and [(bme-daco)Fe]$_2$, the iron atoms are in slightly distorted square pyramidal coordination, where the $N_2S_2$ unit of one ligand is the base and the bridging thiolate sulfur of the second ligand is at the apical position of the pyramid, Figure 1. The $Fe^{II}$ is displaced by 0.59 Å from the mean plane formed by $N_2S_2$ of one ligand in both dimers. This number is not highly significant since there is considerable deviation in the $N_2S_2$ plane due to variations in the axial S donor−Fe−equatorial S-donor angle; these range from 96 to 116°. The $Fe_2S_2$ core is a planar rhombus in both with ∠S−Fe−S of 94.75(7)° and ∠Fe−S−Fe of 85.25(7)° in [(bme*-daco)Fe]$_2$.

The conformation of the bme*-daco ligand in the dimeric complexes reported here is that commonly observed in mononuclear complexes.[1] The two fused metallodiazacyclohexane rings created from the daco framework are in boat/chair conformations. The chair is oriented out and away from the $Fe_2S_2$ core. The boat presents its central methylene group of the metallodiazacyclohexane to the opposite face of the $N_2S_2$ plane and is positioned between the two axial methyl groups of the carbons α to the thiolate sulfurs, Figure 1.

Despite the analogy of the dimeric complexes of the open chain (i.e., nonheterocyclic) $N_2S_2$ ligands shown in Chart 1, the coordination geometries around the iron in the cases of [LFe]$_2$ and [L′Fe]$_2$ are better described as distorted trigonal bipyramid; with one μ-S atom in the basal plane and the other in the axial position, only slightly differing in the Fe−S distances. The Fe−S and Fe−N distances are very similar to those found in [(bme-daco)Fe]$_2$ and [(bme*-daco)Fe]$_2$ and the $Fe_2S_2$ cores are also planar. The Fe−Fe distance in the $Fe_2S_2$ core of [(bme*-daco)Fe]$_2$ is 3.31 Å, much too long for a bond (for which the range is 2.37−3.05 Å) and the S---S core diagonal is 3.59 Å, Table 2. The core Fe−$S_{ax}$ distance is identical to Fe−$S_{ba/br}$ (ba/br = basal/bridge) in [(bme*-daco)Fe]$_2$ and [(bme-daco)-Fe]$_2$ and roughly 0.1 Å longer than the Fe−$S_{ter}$ (ter = terminal).

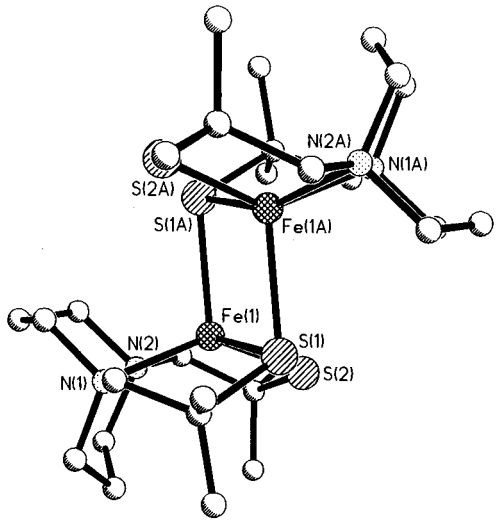


**Figure 1.** Molecular structure as ball-and-stick drawing of [(bme*-daco)Fe]$_2$. The atoms labeled "A" are related by a crystallographic center of symmetry. Selected metric data are given in Table 2, and a full listing is in Supporting Information.

**[(bme*-daco)Fe]$_2$O and [(bme-daco)Fe]$_2$O.** The [(bme*-daco)Fe]$_2$O compound crystallized in the space group $P2_1/c$ with two molecules per unit cell and one cocrystallized toluene molecule; the [(bme-daco)Fe]$_2$O contained two $CH_2Cl_2$ molecules of crystallization and crystallized in a different space group, $P\bar{1}$. As in the iron(II) dimers, the two iron(III) centers of the μ-oxo complexes are in distorted square pyramidal geometries; however, the bridging oxygen is in the apical position, Figures 2 and 3. That is, whereas the complexes containing the $Fe_2S_2$ cores may be described as two edge-bridged square pyramids, the μ-oxo complexes are vertex-bridged with the two $FeN_2S_2$ units related to each other by a center of symmetry at the bridging oxygen. The $Fe^{II}$ dimer structures relate to the (μ-oxo)$Fe^{III}$ complexes by translation of an $FeN_2S_2$ unit so as to bring the iron atoms in line with the oxygen, eclipsing the cis sulfur donors over the nitrogens of the daco donor of the second molecule. The two fused metallodiazacyclooctane structures of each $FeN_2S_2$ unit are substantially the same as in the precursors, i.e., the usual chair/boat conformations persist with the boat conformation on the opposite face of the bridging oxygen in each $FeN_2S_2$ unit. In contrast to the [(bme*-daco)Fe]$_2$ and [(bme-daco)Fe]$_2$ complexes, the $N_2S_2$ planes of both μ-oxo complexes are very regular, with mean deviations of 0.0042 and 0.0644 for [(bme*-daco)Fe]$_2$O and [(bme-daco)-Fe]$_2$O, respectively. In each, the Fe atoms are displaced from the $N_2S_2$ planes toward the bridging oxygen by 0.65 Å for [(bme*-daco)Fe]$_2$O and 0.62 Å for [(bme-daco)Fe]$_2$O. These displacements are in the top 90% of the statistical analysis of data from 30 structures of $(L_4Fe)_2O$ lifted from the Cambridge database which yielded an average out-of-plane distortion of 0.54 Å in a range of 0.296−0.668 Å.[6]

**Table 2.** Comparative Metric Data

| | [(bme-daco)Fe]$_2$ | [(bme*-daco)Fe]$_2$ | [(bme-daco)Fe]$_2$O | [(bme*-daco)Fe]$_2$O |
|---|---|---|---|---|
| Fe−N$_{avg}$ (Å) | 2.255(3) | 2.293(6) | 2.201(6) | 2.219(6) |
| Fe−S$_{ba/ter}$[a] (Å) | 2.346(1) | 2.312(3) | 2.337(2) | 2.331(2) |
| Fe−S$_{ba/br}$[a] (Å) | 2.421(1) | 2.444(2) | 2.335(3) | 2.330(2) |
| Fe−S$_{ax}$ (Å) | 2.417(1) | 2.441(2) | | |
| Fe−O (Å) | | | 1.7742(11) | 1.7798(10) |
| Fe---Fe (Å) | 3.22 | 3.31 | 3.55 | 3.56 |
| ∠E$_{ax}$−Fe−N (avg) (deg) | 102.5(1) | 104.4(2) | 101.1(2) | 100.9(2) |
| ∠E$_{ax}$−Fe−S$_{ba/br}$[a] (deg) | 96.6(1) | 94.75(7) | 111.26(8) | 112.28(9) |
| ∠E$_{ax}$−Fe−S$_{ba/ter}$[a] (deg) | 116.6(1) | 113.89(9) | 109.10(8) | 110.75(9) |
| avg RMS of $N_2S_2$ plane[b] (Å) | 0.189 | 0.1504 | 0.0644 | 0.0042 |
| Fe$N_2S_2$ dome[c] (Å) | 0.59 | 0.59 | 0.62 | 0.65 |

[a] S$_{ba/br}$ = basal/bridging thiolate sulfur, S$_{ba/ter}$ = basal/terminal thiolate sulfur. These designations are not required for the $\mu$-oxo compounds. [b] Average deviation from $N_2S_2$ plane. [c] Dome is defined as the displacement of Fe from the best $N_2S_2$ plane.

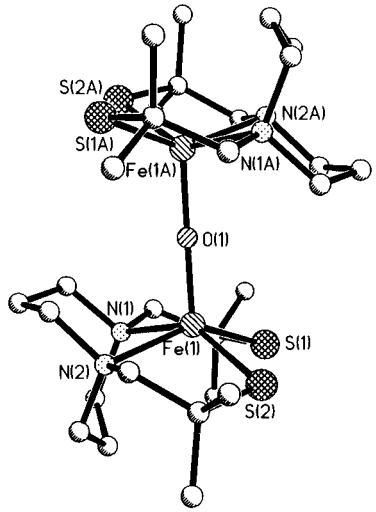


**Figure 2.** Molecular structure as ball-and-stick drawing of [(bme*-daco)Fe]$_2$O. The atoms labeled "A" are related by a crystallographic center of symmetry. Selected metric data are given in Table 2, and a full listing is in Supporting Information.

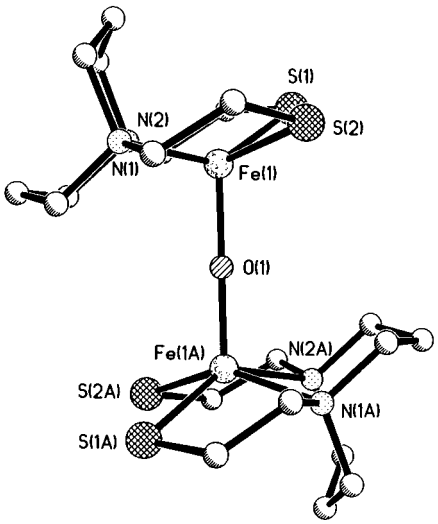


**Figure 3.** Molecular structure as ball-and-stick drawing of [(bme-daco)Fe]$_2$O. The atoms labeled "A" are related by a crystallographic center of symmetry. Selected metric data are given in Table 2, and a full listing is in Supporting Information.

Additional metric data for the complexes are given in Table 2, while comparisons with other examples of $\mu$-oxo complexes are given in Table 3. Included in Table 3 are two Schiff base type ligand derivatives, a porphyrin, and the only $N_2S_2$ type known prior to this work, i.e., [(tsalen)Fe]$_2$O.[7] The Fe−O distances obtained for [(bme*-daco)Fe]$_2$O and [(bme-daco)Fe]$_2$O are in the characteristic range of iron $\mu$-oxo complexes, 1.788−1.820 Å.[6] As shown in Table 3 this distance is independent of the Fe−O−Fe bond angle. Whereas the Fe−O (1.78 Å) and Fe−S (2.33 Å) bond lengths of [(bme-daco)Fe]$_2$O and [(bme*-daco)Fe]$_2$O are similar to those reported for [Fe(tsalen)]$_2$O, the Fe−N (2.22 Å) is longer by ca. 0.20 Å in the former cases. The Fe−Fe (3.56 Å) separation is similar to the complexes listed in Table 3.

**Table 3.** Comparisons of Structural Properties of Pentacoordinate ($\mu$-Oxo)diiron(III) Complexes

| complex[a] | Fe−O (Å) | Fe---Fe (Å) | Fe−O−Fe (deg) | ref |
|---|---|---|---|---|
| [(bme-daco)Fe]$_2$O | 1.7742(11) | 3.55 | 180 | this work |
| [(bme*-daco)Fe]$_2$O | 1.7798(10) | 3.56 | 180 | this work |
| [(tsalen)Fe]$_2$O | 1.78(1) | 3.50(1) | 159(3) | 7 |
| [(salen)Fe]$_2$O | 1.78(1) | 3.39 | 144.6(6) | 16a |
| [(3-*t*-Bu-saltmen)Fe]$_2$O | 1.779(5) | 3.55 | 173.4(3) | 21 |
| [(TPP)Fe]$_2$O | 1.763(1) | 3.5 | 174.5 | 5a |

[a] $H_2$tsalen = *N*,*N*′-ethylenebis(thiosalicylideneimine); $H_2$salen = *N*,*N*′-bis(salicylidene)ethylenediamine; $H_2$(3-*t*-Bu-saltmen) = 2,3-dimethyl-2,3-bis(3-*tert*-butylsalicylideneamino)butane; TPP = α,*β*,*γ*,*δ*-tetraphenylporphine.

The Fe−O−Fe bond angles for pentacoordinate $\mu$-oxo species range from 144 to 180°,[6,16] with ca. 50% of the thirty examined from the CSD, most of these porphyrin-type, being in the 170−180° range. Interestingly, the $N_2S_2$ complexes reported here are also at 180°, while the flat $N_2S_2$ tsalen derivative of Fe is bent, i.e., ∠Fe−O−Fe = 159°. A common phenomenon in the three $N_2S_2$ complexes is that their crystal growth incorporates solvent molecules into their lattices, pyridine in case of [Fe(tsalen)]$_2$O, dichloromethane in case of [(bme-daco)Fe]$_2$O and toluene as well as pyridine, depending on solvent of crystallization, in the case of [(bme*-daco)Fe]$_2$O. The Fe−O−Fe angle and other metric parameters showed insignificant differences in the structures of [(bme*-daco)Fe]$_2$O(py)[17] and [(bme*-daco)Fe]$_2$O(toluene). These results are consistent with studies in the three different [Fe(salen)]$_2$O(solvent)$_x$] structures, in which the three different crystalline environments have a neglible effect on the Fe−O−Fe bond angle.[18] Although all the factors and their combined effects that control the Fe−O−Fe angle have

(16) (a) Davies, J. E.; Gatehouse, B. M. *Acta Crystallogr., Sect. B* **1973**, 1934. (b) Elmali, A.; Atakol, O.; Svoboda, I.; Fuess, H. *Z. Kristallogr.* **1993**, *203*, 275. (c) Elmali, A.; Elerman, Y.; Atakol, O.; Svoboda, I.; Fuess, H. *Z. Kristallogr., Teil B* **1993**, *313*, 48.

(17) X-ray diffracton data were collected at 203 K on a Nicolet R3m/V diffractometer. Crystallographic data are given as *a*, *b*, *c* (Å); *β* (deg); space group, *Z*, Θ range, unique observed reflections, R(*F*), wR($F^2$) (%). [(bme*-daco)Fe]$_2$O·2Py: 11.156 (2), 16.123 (3), 12.967 (3); 110.15(3); $P2_1/c$, 4, 4.22−60.07°, 3445 ($I > 2\sigma(I)$), 6.57 (15.32).

(18) Davies, J. E.; Gatehouse, B. M. *Acta Crystallogr.* **1973**, *B29*, 2651.

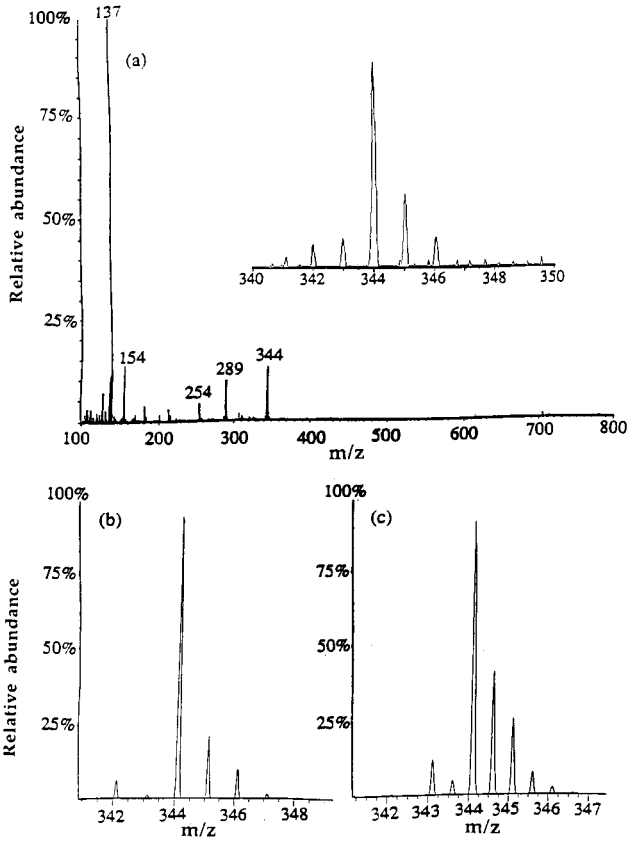


**Figure 4.** (a) Positive ion FAB mass spectrum of $[(bme^*\text{-}daco)Fe]_2$ with expanded parent ion region. (b) Simulated parent ion isotope abundance distribution for $[(bme^*\text{-}daco)Fe]^+$. (c) Simulated parent ion isotope abundance distribution for $[(bme^*\text{-}daco)Fe]_2^{2+}$.

yet to be understood,[19] the fact that the flat ligand (tsalen) produced a smaller angle over the bulky bme-daco and bme*-daco is a bit surprising.

**Mass Spectral Studies.** Positive ion mass spectra of $[(bme^*\text{-}daco)Fe]_2O$ and $[(bme^*\text{-}daco)Fe]_2$ were obtained by electrospray ionization (ESI) and fast atom bombardment (FAB) mass spectrometry. Separate FAB mass spectra were recorded using the matrixes thioglycerol and *m*-nitrobenzyl alcohol (NBA). Both ESI-MS and FAB-MS yielded protonated molecular ion peaks, $[M + H]^+$, for the $[(bme^*\text{-}daco)Fe]_2O$ complex at *m*/*z* 705 and an additional ion peak at *m*/*z* 344 rationalized as half of $[(bme^*\text{-}daco)Fe]_2$, which will be discussed in more detail below. The spectra also contain signals assigned to forms of the ligand, i.e., *m*/*z* = 291, assumed to be the N-protonated dithiol species, $[C_{14}H_{30}N_2S_2 + H]^+$, and *m*/*z* = 289, the N-protonated disulfide, $[C_{14}H_{28}N_2S_2 + H]^+$. Unlike the $[(bme^*\text{-}daco)Fe]_2O$ species, the +FAB mass spectrum of $[(bme^*\text{-}daco)Fe]_2$ in both matrixes does not display a parent ion peak. Figure 4a displays the experimentally determined mass spectrum of $[(bme^*\text{-}daco)Fe]_2O$, with the isotope cluster of *m*/*z* 344 expanded in the insert. Our best interpretation of the base peak signal at *m*/*z* 137 is that it corresponds to the sodium ion adduct of the diazacyclooctane molecule, $[C_6H_{14}N_2 + Na]^+$. The signal observed at *m*/*z* 154 originates from the protonated NBA matrix. Since the ion peak at *m*/*z* 344 may be assigned either to a singly charged monomer, $(bme^*\text{-}daco)Fe^+$ or a doubly charged dimer, $[(bme^*\text{-}daco)Fe]_2^{2+}$, simulation of parent ion isotope abundance distribution were carried out using the IBM PC-compatible program, Isopro, version 2.1.[20] Simulating an instrument resolution of $m/\Delta m = 5000$, the peak distributions shown in Figure 4b and c were calculated assuming $(bme^*\text{-}daco)Fe^+$ and $[(bme^*\text{-}daco)Fe]_2^{2+}$, respectively. The insert of Figure 4a, i.e., the experimentally determined spectrum expanded in the *m*/*z* 344 region and measured at an instrument resolution of 4500, shows no half-integer signals as does the calculated doubly charged dimer (Figure 4c). However, the good match of the simulated distribution of Figure 4b and the experimentally determined distribution of Figure 4a best accounts for the *m*/*z* 344 ion as a singly charged monomer.

In a further, unsuccessful, effort to detect the parent ion of the $[(bme^*\text{-}daco)Fe]_2$, matrix assisted laser desorption time-of-flight mass spectrometry (MALDI-TOF), was performed using a α-cyano-4-hydroxycinnamic acid matrix. While the parent dimer mass was not observed, low-intensity higher aggregates of *m*/*z* 801, 803, and 991 appeared, in addition to the ions which were observed by the first two techniques. Isotopic distribution patterns of the signals indicate the presence of iron(s) in the cluster(s). In this connection, it is noteworthy that electron impact (EI) mass spectral studies by Lippard and co-workers on $[FeL]_2$ and $[FeL']_2$, Chart 1, showed minor signals at *m*/*z* 524 and 552, respectively, for the parent dimers, as well as at *m*/*z* 266 and 276, which correspond to the monomeric units FeL and FeL′.[8] Thus, in all four iron(II) $N_2S_2$ complexes shown in Chart 1, the monomeric iron units are prominent species in the mass spectra. Unlike the mass spectra of $[(bme\text{-}daco)Fe]_2$ and $[(bme^*\text{-}daco)Fe]_2$, the spectra of $[FeL]_2$ and $[FeL']_2$ do not have signals which correspond to the respective free ligands.[8]

**Electronic and Vibrational Spectra.** The electronic spectra of all the pentacoordinate iron complexes of this study display three intense absorptions in the same region, ca. 300, 400, and 500 nm. The differences between pentacoordinate iron(II) in $N_2S_3$ coordination environment of the dimer vs the $N_2S_2O$ of the $Fe^{III}$ μ-oxo compounds are minor and not easily rationalized. The electronic spectra of the latter are also similar to $Fe^{III}$ in $N_2O_3$ coordination.[21] Likewise the vibrational frequency due to the Fe−O−Fe asymmetric stretch at 821 and 841 $cm^{-1}$, for $[(bme\text{-}daco)Fe]_2O$ and $[(bme^*\text{-}daco)Fe]_2O$, respectively, are similar to the salen and porphyrin μ-oxo derivatives.[21]

**Magnetic Properties and Electron Paramagnetic Resonance Results.** The small magnetic moment of 1.32 $\mu_B$ per iron for $[(bme^*\text{-}daco)Fe]_2O$ which was determined by the Evans' method[22] at room temperature is reasonably explained in terms of antiferromagnetic interactions between the paired irons. This value is comparable with those of well-known μ-oxo-complexes with antiferromagnetic interaction between the ferric sites, such as (μ-oxo)bis((phthalocyaninato)iron(III)) (1.4−1.6 $\mu_B$)[5d] and $[Fe(cbpN)]_2O$ (1.1 $\mu_B$),[23] but is smaller than those[21] of $[Fe(salen)]_2O$ (1.92 $\mu_B$) and $[Fe(3\text{-}t\text{-}Bu\text{-}saltmen)]_2O$ (1.88 $\mu_B$) which have ∠Fe−O−Fe of 144.6(6) and 173.4(3)°, respectively. The antiferromagnetic character of $[(bme^*\text{-}daco)Fe]_2O$ was also confirmed by the electron paramagetic resonance results. As a

(19) (a) Murray, K. S. *Coord. Chem. Rev.* **1974**, *12*, 1. (b) Kurtz, D. M. *Chem. Rev.* **1990**, *90*, 585.

(20) Senko, M. W.; National High Magnetic Field Laboratory, 1800 E. Paul Dirac Drive, Tallahassee, FL 32310. This IBM PC-compatible program utilizes the Yeargy Algorithm (Yergey, J. A. *Int. J. Mass Spectrom. Ion Phys.* **1983**, *52*, 337−349) to calculate theoretical isotope distributions which are reported in a tabular and/or graphic output consisting of Gaussian peak profiles that are dependent upon a user-selected input of mass spectrometer resolution.

(21) Mukherjee, R. N.; Stack, T. D. P.; Holm, R. H. *J. Am. Chem. Soc.* **1988**, *110*, 1850.

(22) (a) Evans, D. F. *J. Chem. Soc.* **1959**, 2003. (b) Grant, D. H. *J. Chem. Educ.* **1995**, *72*, 39.

(23) Mockler, G. M.; Jersey, J. de.; Zerner, B.; O'Connor, C. J.; Sinn, E. *J. Am. Chem. Soc.* **1983**, *105*, 1891.

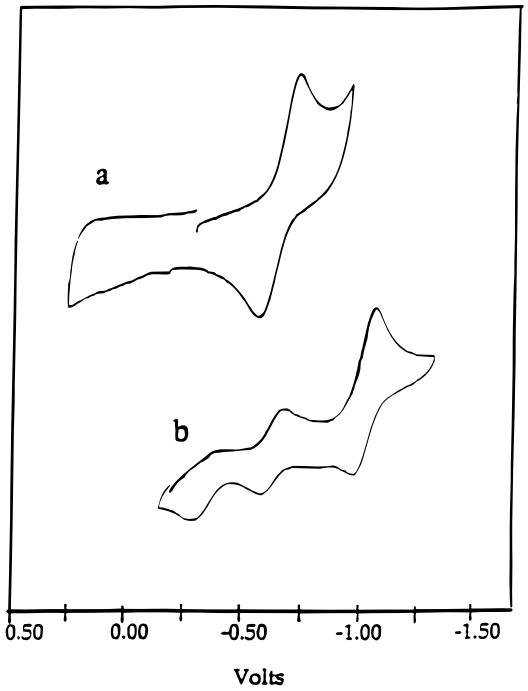


**Figure 5.** Cyclic voltammograms of 2.5 mM solutions of (a) [(bme*-daco)Fe]$_2$ and (b) [(bme*-daco)Fe]$_2$O in 0.1 mM TBAHFP/$CH_3CN$ with a gold working electrode at a scan rate of 150 mV/s. All potentials are scaled to NHE using $Cp_2Fe^+/Cp_2Fe$ as internal standard ($E_{1/2} = 0.40$ mV).[11]

solid powder as well as in frozen acetonitrile solution, [(bme*-daco)Fe]$_2$O is EPR silent. The EPR spectrum of a frozen acetonitrile solution of one-electron reduced [(bme*-daco)Fe]$_2$O was measured at 10 K. A rhombic spectrum with $g_1 = 2.03$, $g_2 = 1.99$, and $g_3 = 1.94$, typical of low-spin Fe(III) ($S = {}^1/_2$) was observed. The spectrum of a wider field scan contains an additional signal at $g = 4.29$; similar signals have been reported for high-spin monomeric $Fe^{III}$ complexes.[24]

**Electrochemical Studies.** Figure 5 shows cyclic voltammograms of [(bme*-daco)Fe]$_2$ and [(bme*-daco)Fe]$_2$O in acetonitrile solutions. The former shows a quasireversible one-electron reduction at −0.73 V, which is assigned to the $Fe^{II}Fe^{II}/Fe^{II}Fe^{I}$ couple. Further scanning toward more negative potentials resulted in a rise of the cathodic current due to decomposition of the $Fe^{II}Fe^{I}$ species. For [(bme*-daco)Fe]$_2$O, the voltammogram shows two electrochemically reversible one electron reductions at $E_{1/2} = -0.64$ and −1.05 V and an irreversible oxidation at −0.30 V. The two reversible reductions of [(bme*-daco)Fe]$_2$O are assigned to $Fe^{III/III}/Fe^{III/II}$ and $Fe^{III/II}/Fe^{II/II}$, respectively; we have assigned a similar irreversible wave to thiolate oxidation in the case of (bme*-daco)Ni.[25]

Assignments for the stepwise iron-based reductions of the complex are shown in eqs 2−4. From the separations of the

$$Fe^{III}-O-Fe^{III} + e^- \rightleftharpoons Fe^{II}-O-F^{III},\ E_1 = -635\ \text{mV} \quad (2)$$

$$Fe^{II}-O-Fe^{III} + e^- \rightleftharpoons Fe^{II}-O-F^{II},\ E_2 = -1054\ \text{mV} \quad (3)$$

$$Fe^{II}-O-Fe^{II} + Fe^{III}-O-F^{III} \rightleftharpoons 2Fe^{II}-O-Fe^{III} \quad (4)$$

first and second reduction potentials of the [(bme*-daco)Fe]$_2$O, the comproportionation constant of reaction 4 may be calculated: $E_2 - E_1 = (RT/F)\ln K_{com}$, and $K_{com} = 5.8 \times 10^{10}$. Despite this large value and suggestion of stability, our efforts to isolate the mixed valent state of $Fe^{III}OFe^{II}$ were unsuccessful. This $K_{com}$ value is slightly lower than one obtained for a $\mu$-oxo high-spin iron(II)−low-spin iron(III) complex of a nonadentate polypyridine binucleating ligand, which was isolable and characterized.[24]

**Scheme 2**

$$[(bme^*\text{-}daco)Fe^{II}]_2 \rightleftharpoons 2[(bme^*\text{-}daco)Fe^{II}]$$

$$[(bme^*\text{-}daco)Fe^{II}]_2 + O_2 \longrightarrow (bme^*\text{-}daco)Fe^{III}-O_2-Fe^{III}(bme^*\text{-}daco)$$

$$(bme^*\text{-}daco)Fe^{III}-O_2-Fe^{III}(bme^*\text{-}daco) \longrightarrow 2\,(bme^*\text{-}daco)Fe^{IV}-O$$

$$(bme^*\text{-}daco)Fe^{IV}-O \xrightarrow{[(bme^*\text{-}daco)Fe^{II}]} (bme^*\text{-}daco)Fe^{III}-O-Fe^{III}(bme^*\text{-}daco)$$

**Mechanistic Considerations.** Although there are many $\mu$-oxo binuclear complexes of iron(III), prior to this work few were known to arise from an iron dimer precursor. A notable exception is the recently elucidated mechanism of iron(II) precursors reaction with $O_2$ which lead to tetrairon bis($\mu$-oxo) species.[26] This mechanism involves an intramolecular binding and activation of $O_2$ which subsequently reacts with a diiron precursor, clearly inappropriate in our system. The widely accepted mechanism for the oxidation of iron(II) porphyrins to iron(III) $\mu$-oxo species is applicable to the chemistry described herein,[27] assuming a dimer−monomer preequilibrium precedes the binding of molecular oxygen and the production of a ferryl intermediate, as outlined in Scheme 2.

The sluggish reactivity of the intact or premade [(bme*-daco)-Fe]$_2$ dimer is consistent with the tight $Fe_2S_2$ core established by the crystallographic data. However the observation of the $FeN_2S_2$ monomer in the softest of mass spectral ionization techniques suggests the possibility of dimer dissociation. On the other hand, attempts to disrupt the dimer by use of the solvent pyridine resulted in no more rapid $O_2$ uptake. Crystals obtained from this experiment simply included a pyridine of crystallization with the dimeric molecule.[17]

Alternatively, an intriguing mechanistic possibility is suggested from early work of Lippard et al., in which $NO^+$ was demonstrated to undergo an oxidative addition to the $[FeL]_2$ complex shown in Chart 1.[28] The reaction product, characterized by X-ray crystallography, contained an $\eta^1$-bridging NO and also retained the ($\mu$-SR)$_2$ bridges in the binuclear species. In fact, Lippard et al. suggested similar species could be possible intermediates for $O_2$uptake in bimetallic biological systems.[28] Hence, this "hinge opening" mechanistic possibility could be appropriate for the uptake of $O_2$ by [(bme*-daco)Fe]$_2$ giving rise to a similar Fe($\mu$,$\eta^1$-$O_2$)Fe intermediate as shown below.

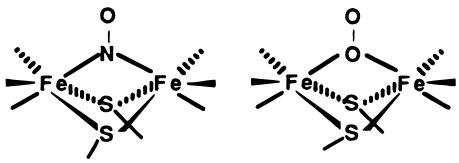


Clearly the elegant approach to distinguish these mechanisms would utilize crossover experiments involving isotopically labeled, $d_{16}$-bme*-daco, with expectations that the mixtures of $d_{32}$-[(bme*-daco)Fe]$_2$ and $d_0$-[(bme*-daco)Fe]$_2$ when reacted

(24) Maeda, Y.; Kawano, K.; Oniki, T. *J. Chem. Soc., Dalton Trans.* **1995**, 3533.
(25) Buonomo, R. M.; Font, I.; Maguire, M. J.; Reibenspies, J. H.; Tuntulani, T.; Darensbourg, M. Y. *J. Am. Chem. Soc.* **1995**, *117*, 963.
(26) Feig, A. L.; Becker, M.; Schindler, S.; van Eldik, R.; Lippard, S. J. *Inorg. Chem.* **1996**, *35*, 2590.
(27) Chin, D.-H.; La Mar, G. N.; Balch, A. L. *J. Am. Chem. Soc.* **1980**, *102*, 4344 and references therein.
(28) Rabinowitz, H. N.; Karlin, K. D.; Lippard, S. J. *J. Am. Chem. Soc.* **1977**, *99*, 1420.

with $O_2$ should show scrambling if the mechanism is that in Scheme 2, while the hinge opening process would maintain label integrity. Such experiments are yet to be done.

The discrepancy of rates of formation of the μ−oxo product from the premade dimer vs its origination from synthesis components $Fe(acac)_3$, $H_2$bme*-daco and $O_2$, finds simplest explanation in (a) interception of the $Fe^{II}$ monomer by $O_2$ before the stable dimers are formed; or (b) $O_2$ activation by the electrophilic $Fe(acac)_3$ or H-bonding from the free thiol ligand ($pK_a$ in range of 9−12) represented by "E" in eq 5. Unfortu-

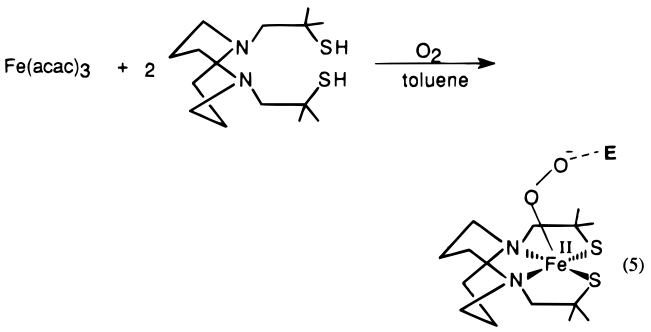


(5)

nately these reasonable expectations were not supported by control experiments. Attempts to enhance the reactivity rates of the dimer with $O_2$ have included deliberate addition of $Fe(acac)_3$ and addition of H-bonding solvents, methanol and water. These did not significantly alter the reaction rate.

**Comments and Conclusions.** The [(bme*-daco)Fe]$_2$O and [(bme-daco)Fe]$_2$O complexes are, to our knowledge, the first fully characterized μ-oxo iron(III) complexes in the presence of thiolate sulfur donors. We saw no evidence for sulfur-based oxygenates as stable products in the reaction of the iron dithiolates with $O_2$; however, the reactivity of [(bme-daco)Fe]$_2$O with $O_2$ implicates S-based $O_2$ reactivity in the μ-oxo Fe(III) complex. In fact the [(bme*-daco)Fe]$_2$O and [(bme-daco)Fe]$_2$O complexes differ substantially in their air sensitivity, the former being air stable while the latter, as well as its dimeric precursor, reacted with $O_2$, producing uncharacterized decomposition products, presumably ligand disulfide. The latter result is consistent with previous observations of uncharacterized oxygen degradation in the Lippard et al. [FeL]$_2$ and [FeL′]$_2$ complexes, Chart 1.[8] We conclude that the steric hindrance provided by gem-dimethyl groups of the bme*-daco ligand is sufficient to prevent disulfide formation and loss of metal upon reaction with $O_2$.

**Acknowledgment.** Financial support from the National Science Foundation (CHE 94-15901) for this work, NSF CHE-8705697 to the TAMU Mass Spectrometry facility, CHE-8513273 for the X-ray diffractometer and crystallographic computing system and contributions from the R. A. Welch Foundation are gratefully acknowledged. We thank Dr. Barbara P. Wolf for the mass spectra measurements.

**Supporting Information Available:** Tables of crystallographic data collection parameters, atomic coordinates and equivalent isotropic displacement parameters, complete listings of bond lengths and bond angles, anisotropic displacement parameters, and packing diagrams for complexes [(bme*-daco)Fe]$_2$, [(bme*-daco)Fe]$_2$O and [(bme-daco)Fe]$_2$O (30 pages). Ordering information is given on any current masthead page.

IC980475F